Wind and Structures, Vol. 14, No. 5 (2011) 465-480
DOI: http://dx.doi.org/10.12989/was.2011.14.5.465

Stabilized finite element technique and its application for turbulent flow with high Reynolds number

Cheng Huang, Bao Yan, Dai Zhou* and Jinquan Xu

School of Naval Architecture, Ocean and Civil engineering, Shanghai Jiao Tong University, Shanghai 200240, China

(Received December 11, 2009, Accepted May 1, 2011)

Abstract. In this paper, a stabilized large eddy simulation technique is developed to predict turbulent flow with high Reynolds number. Streamline Upwind Petrov-Galerkin (SUPG) stabilized method and three-step technique are both implemented for the finite element formulation of Smagorinsky sub-grid scale (SGS) model. Temporal discretization is performed using three-step technique with viscous term treated implicitly. And the pressure is computed from Poisson equation derived from the incompressible condition. Then two numerical examples of turbulent flow with high Reynolds number are discussed. One is lid driven flow at $Re = 10^5$ in a triangular cavity, the other is turbulent flow past a square cylinder at $Re = 22000$. Results show that the present technique can effectively suppress the instabilities of turbulent flow caused by traditional FEM and well predict the unsteady flow even with coarse mesh.

Keywords: large eddy simulation; finite element method; high Reynolds number; Streamline Upwind Petrov-Galerkin; subgrid-scale model.

1. Introduction

Among a number of existing numerical techniques for predicting turbulent flow, large eddy simulation (LES) appears to be one of the most promising approaches (Itoh and Tamura 2008, Jimenez *et al*. 2008, Uchida and Ohya 2003). In LES, the fluctuating motions of turbulence can be computed exactly except for the eddy smaller than the grid size. Early LES computations were based on the Smagorinsky model (SM) for the sub-grid scales (SGS) (Smagorinsky 1963). Potential of this scheme has been clearly demonstrated by Deardorff (1970). And some other SGS models have been proposed such as the scale similarity model (Bardina *et al.* 1980) and the dynamic sub-grid scale model (Germano *et al.* 1991).

For the advantages of dealing with complex geometry and boundary conditions, finite element method (FEM) has been widely used for the predictions of various fluid dynamic problems. However, classic Galerkin FEM meets great problem when applied to solve fluid flow with high Reynolds number as it is mentioned by Collis and Heinkenschloss (2002). In order to overcome this drawback, some stabilized finite element formulations have been developed by many researchers for decades. Among them, Streamline Upwind Petrov-Galerkin (SUPG) method is famous which was proposed by Brooks and Hughes (1982) and further developed by Hughes *et al.* (1986) and

* Corresponding Author, Professor, E-mail: zhoudai@sjtu.edu.cn

Tezduyar (2007).

Besides, there are some other stabilized methods such as Galerkin least Square techniques (Hughes *et al.* 1989, Franca and Frey 1992), characteristic Galerkin method (Zienkiewicz and Codina 1995, Bao *et al*. 2010a, b) and finite calculus method (Oñate 1998). Based on the Taylor-Galerkin method developed by Donea *et al.* (1984) and Selmin *et al.* (1985), the three-step finite element method developed by Jiang and Kawahara (1993) has been proved to be effective, stable and accurate for turbulent flow with high Reynolds number.

Recently, a 2-D Streamline Upwind Petrov/Galerkin (SUPG) finite element model was developed for coupled convection-diffusion equation in the feed channel (Ma *et al*. 2004). Pain and Eaton (2006) present a space-time Streamline Upwind Petrov-Galerkin formulation for the time-dependent Boltzmann transport equation. Ramakrishnan and Collis (2006) obtain good numerical results with variational multiscale method for large-eddy simulation. Buchan *et al*. (2008) present a new multiscale radiation transport method of the Boltzmann transport equation. Becker and Vexler (2007) present a stabilization scheme on coarse mesh in the convection dominated case. And Heinkenschloss and Leykekhman (2008) derive local error estimates for the discretization of optimal control problems using the Streamline Upwind Petrov/Galerkin (SUPG) stabilized finite element method.

In this paper, turbulent flow with high Reynolds number is concerned. Because the weak form of the finite element formulations added with the SUPG stabilized term has better stability properties with strongly consistent stabilization (Collis and Heinkenschloss 2002), the formulation of Smagorinsky SGS model with SUPG stabilized method is applied. The theory and efficiency of the SUPG stabilized term in the weak form are introduced and discussed by Brooks and Hughes (1982). The same order interpolation for the velocity and pressure is employed for the spatial discretization, and the three-step technique is applied for the temporal discretization where viscous term is treated implicitly. The Poisson equation is derived from the incompressible condition.

For the verification of present method, the numerical examples of lid driven flow in a triangular cavity at $Re = 10^5$ and flow past a square cylinder at $Re = 22000$ are operated. Results show that present method is stable and efficient for the simulation of fluid flow with high Reynolds number.

2. Governing equations

2.1 LES governing equations

The governing equations of Smagorinsky SGS model for incompressible flow are as follows (Smagorinsky 1963)

$$u_{i,i} = 0 \tag{1}$$

$$u_{i,t} + u_j u_{i,j} = -(p/\rho + 2k/3)_{,i} + [(\nu + \nu_t)(u_{i,j} + u_{j,i})]_{,j} \tag{2}$$

where $\nu_t = (C_S h)^2 (2S_{ij}^2)^{0.5}$, $S_{ij} = (u_{i,j} + u_{j,i})/2$, $h = (h_1 h_2 h_3)^{1/3}$ for 3D and $(h_1 h_2)^{1/2}$ for 2D, and $k = (\nu_t/(C_k h))^2$. u and p are the velocity and pressure respectively, t is the time, ν is $1/Re$ as kinematic viscosity, Re is Reynolds number, ν_t is the turbulent eddy viscosity, S_{ij} is the strain rate tensor, k is the SGS turbulent kinetic energy, h_1, h_2, h_3 are the element volume sizes in three directions, ρ is the density of fluid. Constants used here, $C_S = 0.15$, $C_k = 0.094$ are suggested by Murakami and Mochida (1995).

2.2 Finite element formulations for LES

The weak form of the momentum equation can be actualized via Eq.(2) multiplying the velocity test function and added with SUPG stabilized term as follows (Brooks and Hughes 1982)

$$\int_{\Omega}[\delta u_i(u_{i,t} + u_j u_{i,j}) + \sigma_{ij}\delta u_{i,j}]d\Omega - \int_{\Gamma^h}\sigma_{ij}n_j\delta u_i d\Gamma + \sum_{e=1}^{n_{el}}\int_{\Omega^e}\tau_{\mathrm{SUPG}}u_j\delta u_{i,j}\left(\frac{\partial u_i}{\partial t} + u_j u_{i,j} - \sigma_{ij,j}\right)d\Omega = 0 \tag{3}$$

where n_{el} is the number of elements, δu_i is the velocity test function, n_j is the normal unit vector of the computational boundary Γ, Ω is the computational domain, Ω^e is the element domain and σ_{ij} is the stress tensor given by

$$\sigma_{ij} = -(p/\rho + 2k/3)\delta_{ij} + (\nu + \nu_t)(u_{i,j} + u_{j,i}) \tag{4}$$

and the stabilized parameter τ_{SUPG} is defined as follow from Dettmer and Peric (2006)

$$\tau_{SUPG} = \frac{h^e}{2u^e\rho}z \qquad z = \frac{\beta_1}{\sqrt{1 + \left(\frac{\beta_1}{\beta_2 Re^e}\right)^2}} \qquad Re^e = \frac{u^e h^e}{2\nu} \tag{5}$$

where h^e, u^e and Re^e represent the characteristic element size, convective velocity and the Reynolds number of an element respectively. And β_1 defines the limits of z as Re^e near to infinite and β_2 define the derivative dz/dRe^e at $Re^e = 0$. In this work, $\beta_1 = 1$ and $\beta_2 = 1/3$ have been obtained, and the characteristic element size is defined as the diameter of a circle which area is equal to the element area.

3. Numerical schemes

3.1 Spatial discretization

The spatial discretization of Eq.(3) is performed with the velocity and pressure both employing the same order interpolation. Thus the trial function and the test function for velocity and pressure are both expressed as Φ_I, and the velocity and pressure of an element are described as

$$u_i = \Phi_I u_{iI} \qquad p = \Phi_I p_I \tag{6}$$

where u_{iI} is the i directional velocity of node I, p_I is the pressure of node I.

Substituting Eq.(6) into Eq.(3), the finite element formulation for momentum equation is expressed as

$$M_{IJ}\frac{\partial u_{iJ}}{\partial t} + N_{IJ}u_{iJ} - G_{iIJ}p_J + H_{iI} + D_{IJ}u_{iJ} - B_{iI} = 0 \tag{7}$$

where the basis matrices of elements are obtained as

$$M_{IJ} = \int_{\Omega} \Phi_I \Phi_J d\Omega + \tau_{SUPG} \int_{\Omega} \Phi_{I,j} \Phi_J \Phi_K u_{jK} d\Omega \tag{8}$$

$$N_{IJ} = \int_{\Omega} \Phi_I u_{iK} \Phi_K \Phi_{J,i} d\Omega + \tau_{SUPG} \int_{\Omega} \Phi_{I,j} \Phi_L u_{jL} \Phi_K u_{jK} \Phi_{jJ} d\Omega \tag{9}$$

$$G_{iIJ} = \frac{1}{\rho} \int_{\Omega} \Phi_{I,i} \Phi_J d\Omega - \tau_{SUPG} \frac{1}{\rho} \int_{\Omega} \Phi_{I,j} \Phi_K u_{jK} \Phi_{J,i} d\Omega \tag{10}$$

$$H_{iI} = (\nu + \nu_t) \int_{\Omega} \Phi_{I,j} \Phi_{J,i} u_{jJ} d\Omega - \frac{2}{3} k \int_{\Omega} \Phi_{I,i} d\Omega \tag{11}$$

$$D_{IJ} = (\nu + \nu_t) \int_{\Omega} \Phi_{I,j} \Phi_{J,j} d\Omega \tag{12}$$

$$B_{iI} = \int_{\Gamma} \Phi_I \sigma_{ij} n_j d\Gamma \tag{13}$$

3.2 Temporal discretization

Three-step technique is applied here for the temporal discretization with viscous term treated implicitly and the formulation of the momentum equation at each step is expressed as below (Jiang and Kawahara 1993)

$$M^n_{IJ} \frac{u_{iJ}^{n+\frac{1}{3}} - n^n_{iJ}}{\Delta t/3} = -N^n_{IJ} n^n_{iJ} + G^n_{iIJ} P^n_J - H^n_{IJ} - u_{IJ}^{n+\frac{1}{3}} u_{iJ}^{n+\frac{1}{3}} + B^n_{iI} \tag{14}$$

$$M_{IJ}^{n+\frac{1}{3}} \frac{u_{iJ}^{n+\frac{2}{3}} - u_{iJ}^{n+\frac{1}{3}}}{\Delta t/3} = -N_{IJ}^{n+\frac{1}{3}} u_{iJ}^{n+\frac{1}{3}} + G_{iIJ}^{n+\frac{1}{3}} P^n_J - H_{iI}^{n+\frac{1}{3}} - D_{IJ}^{n+\frac{2}{3}} u_{iJ}^{n+\frac{2}{3}} + B_{iI}^{n+\frac{1}{3}} \tag{15}$$

$$M_{IJ}^{n+\frac{2}{3}} \frac{u_{iJ}^{n+1} - u_{iJ}^{n+\frac{2}{3}}}{\Delta t/3} = -N_{IJ}^{n+\frac{2}{3}} u_{iJ}^{n+\frac{2}{3}} + G_{iIJ}^{n+\frac{2}{3}} P_J^{n+1} - H_{iI}^{n+\frac{2}{3}} - D_{IJ}^{n+1} u_{iJ}^{n+1} + B_{iI}^{n+\frac{2}{3}} \tag{16}$$

where Δt represents the length of time increment, the superscripts of n, $n+\frac{1}{3}$ and $n+\frac{2}{3}$ denote steps of time increment respectively.

3.3 Finite element formulation for pressure equation

Before calculating the velocity u_i^{n+1} from Eq.(16), the pressure p^{n+1} has to be confirmed. By taking the divergence of both sides of Eq.(2) and considering the incompressible condition of $u_{i,j}^{n+1} = 0$, the Poisson equation is obtained as

$$\frac{p^{n+1}_{,ii}}{\rho} = \frac{u^n_{i,i}}{\Delta t} - \left(u_j^{n+\frac{1}{2}} u_{i,j}^{n+\frac{1}{2}}\right), i + (\nu + \nu_t)\left(u_{i,j}^{n+\frac{1}{2}} + u_{i,j}^{n+\frac{1}{2}}\right), ij - \frac{2}{3} k^n_{,ii} \tag{17}$$

where $u^{n+\frac{1}{2}} = \left(u^{n+\frac{1}{3}} + u^{n+\frac{2}{3}}\right)/2$

Using the trial function and the test function of Eq.(6), and considering k and ν_t evaluated at the center of element, the finite element formulation for pressure is shown as

$$S_{IJ}p_J^{n+1} = Q_{iIJ}u_{iJ}^n - R_{iIJ}u_{iJ}^{n+\frac{1}{2}} - T_I \tag{18}$$

where the basis matrices of element are obtained as

$$S_{IJ} = \frac{1}{\rho}\int_{\Omega}\Phi_{I,i}\Phi_{J,i}d\Omega \tag{19}$$

$$Q_{iIJ} = \frac{1}{\Delta t}\int_{\Omega}\Phi_I\Phi_{J,i}d\Omega \tag{20}$$

$$R_{iIJ} = \int_{\Omega}\Phi_{I,j}\Phi_J\Phi_{K,i}u_{jK}^{n+\frac{1}{2}}d\Omega \tag{21}$$

$$T_I = \frac{1}{\Delta t}\int_{\Gamma}\Phi_I(u_i^{n+1} - u_i^n)n_i d\Gamma \tag{22}$$

4. Numerical examples

4.1 Lid driven flow in a triangular cavity at Re = 10^5

In this section, a lid driven flow of $Re = 10^5$ in a triangular cavity is considered. A horizontal velocity ($U = 1.0$) is prescribed on the top side which length $H = 1.0$, while the no-slip boundary condition is imposed on the other two sides. Biconjugate gradient solver is employed to solve this system.

The mesh system and boundary conditions of computational domain are shown in Fig. 1, where 1310 unstructured elements are used to discretize the triangular cavity and the time increment is

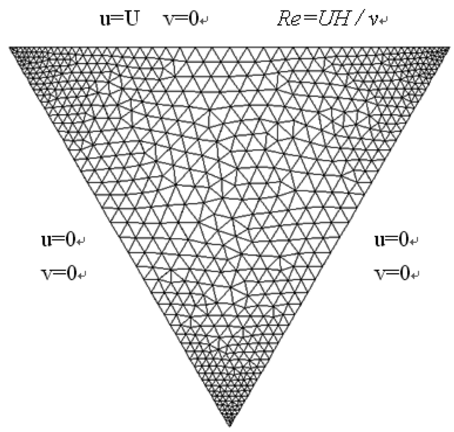

Fig. 1 Finite element mesh and boundary conditions

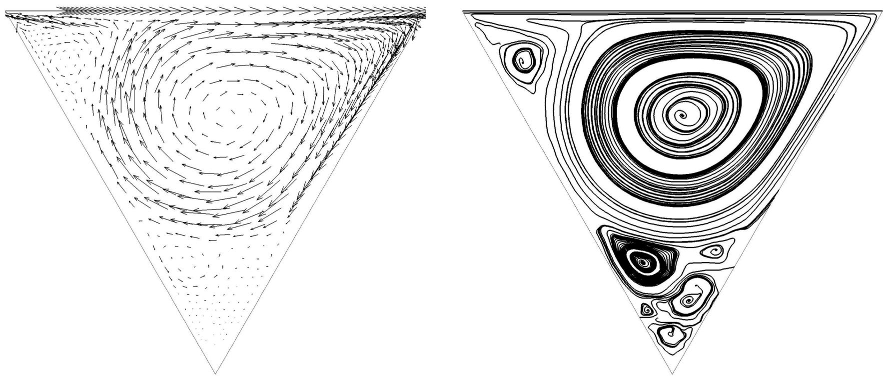

(a) velocity vector (b) streamline

Fig. 2 Velocity vector and streamline of fluid flow at t =100 for Re = 10^5

0.01 for this prediction.

Figs. 2(a) and (b) show the velocity vector and the streamline distribution in the triangular cavity by present computation at $t = 100$ respectively. There is one main vortex in the middle due to the boundary conditions of this problem. And in the left and down corners there are small and disordered vortices showing the flow characteristics by LES.

Figs. 3, 4 and 5 show the horizontal velocity (u) field, vertical velocity (v) field and pressure (p) field at $t = 100$ predicted by present method and predicted without SUPG respectively. It can be seen that the velocities and pressure fields by present method are very fluent, but those without SUPG exist obvious numerical oscillations, showing that present method has good stabilization for velocities and pressure fields than the normal method without stabilization strategy.

4.2 Turbulent flow past a square cylinder at Re = 22000

Two dimensional (2D) turbulent flow past a square cylinder under $Re = 22000$ is simulated. The

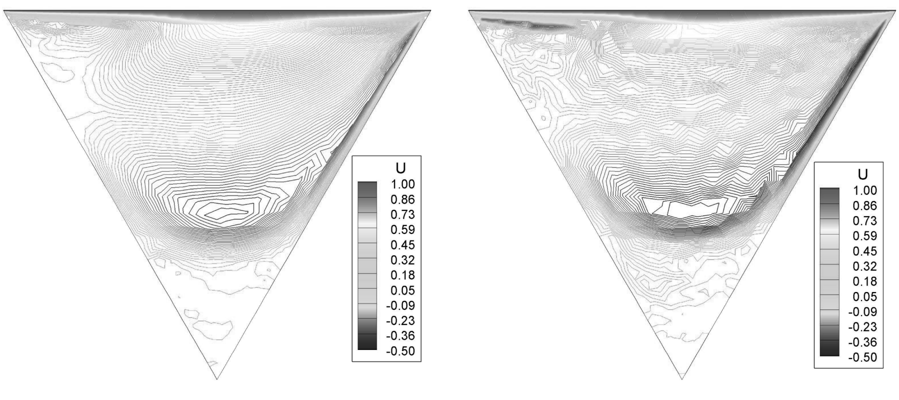

(a) Present method (b) LES without SUPG

Fig. 3 Horizontal velocity (u) field at t = 100 for Re = 10^5

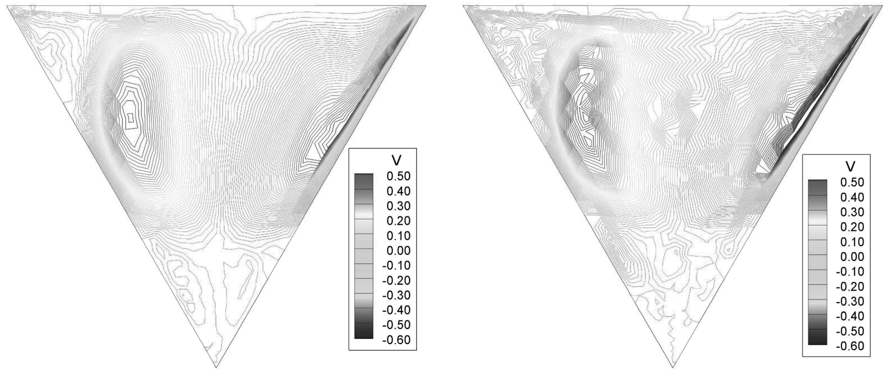

(a) Present method (b) LES without SUPG

Fig. 4 Vertical velocity (v) field at $t = 100$ for $Re = 10^5$

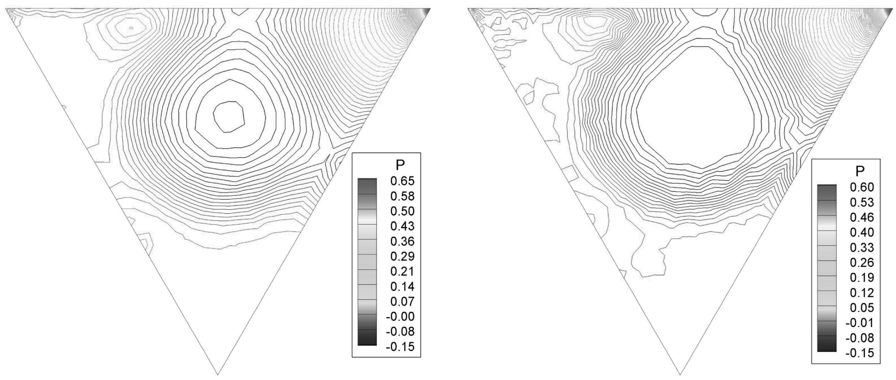

(a) Present method (b) LES without SUPG

Fig. 5 Pressure (p) field at $t = 100$ for $Re = 10^5$

same 2D and 3D numerical simulations are also predicted by Hasebe and Nomura (2009), as well as Tutar and Celik (2007). The computational domain, boundary conditions and mesh system of present study are shown in Fig. 6. The characteristic velocity (U) in streamwise direction from left inlet and the characteristic length (H) of the square cylinder are both unit value. The distances upstream and downstream of the square cylinder are $5H$ and $10H$ respectively while the width of the region is $7H$. Uniform mesh system with 5027 rectangle elements, which grid size is about 0.143, are used to discretize the computational domain. The uniform and coarse meshes applied here are for the verification of the stabilization and the capability of yielding accurate prediction by present method. And the time increment of 0.01 and total time of 500 are applied for the computation.

4.2.1 Flow patterns analysis

Flow past square cylinder at $Re = 22000$ is visualized by velocity vector, streamline distribution, and vorticity distribution. Then streamwise (x-directional) velocity (u) fields, lateral (y-directional)

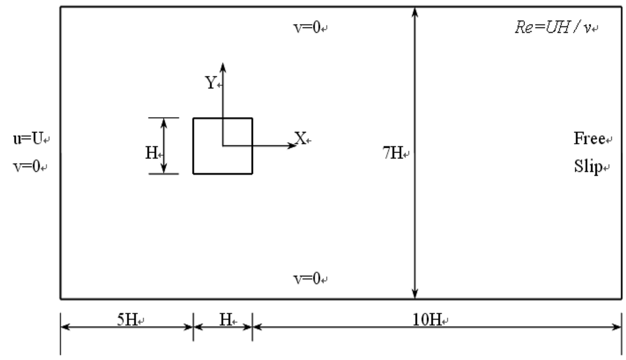

(a) geometry and boundary conditions

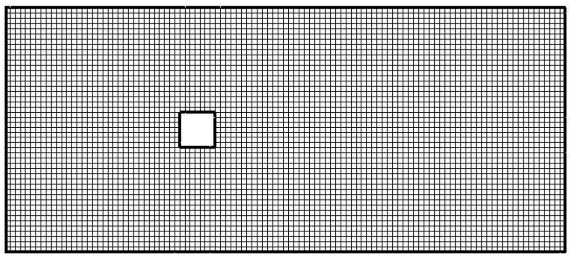

(b) mesh

Fig. 6 Geometry, boundary conditions and mesh

velocity (v) fields and pressure fields (p) based on the present prediction and the prediction without SUPG are compared to verify the stability effect.

Figs. 7(a), (b) and (c) show the velocity vector near the cylinder, the streamline distribution and vorticity distribution of flow by present computation at $t = 100$ respectively. And Figs. 8, 9 and 10 show the comparison of streamwise velocity (u) field, lateral velocity (v) field and pressure (p) field computed by present method and by the method without SUPG at $t = 100$ respectively.

It can be seen that the separation of flow happens at the upwind corners where the strong vorticities are produced, spread downstream and form vortex street behind the square cylinder with clockwise and anticlockwise vorticity alternately. And the positive pressure exists on the front face of the square cylinder, and the minus pressure (suction) exists on the side and rear faces of the square cylinder.

From Figs. 8, 9 and 10, it can be observed that the present method gains stable flow fields, while the results without SUPG have obvious numerical oscillations, showing that the present method has good stabilization for simulation of fluid fields even with coarse elements.

4.2.2 Aerodynamic forces analysis

The periodic vortex shedding phenomena by separated flow past bluff body will cause fluctuation of forces. Some of the parameters are used to characterize the flow behavior, such as the drag coefficient C_d, lift coefficient C_l and the Strouhal number S_t defined as

$$C_d = F_d/(0.5\rho U^2 H) \tag{23}$$

$$C_1 = F_1/(0.5\rho U^2 H) \tag{24}$$

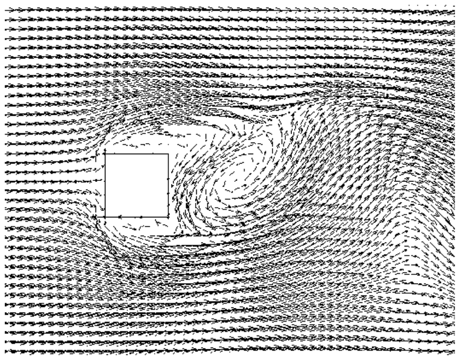

(a) velocity vector of local fluid domain

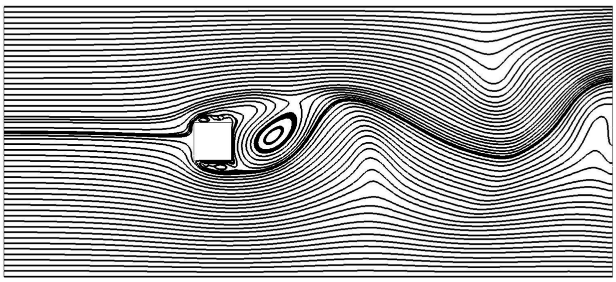

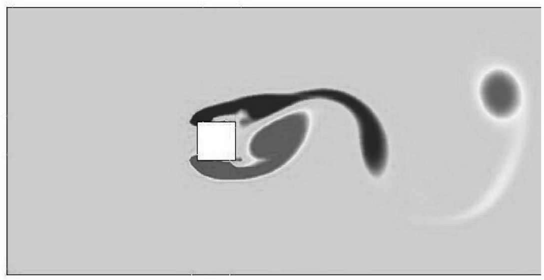

(b) streamline distribution (c) vorticity distribution

Fig. 7 Velocity vector and streamline of fluid flow at t =100 for Re = 22000

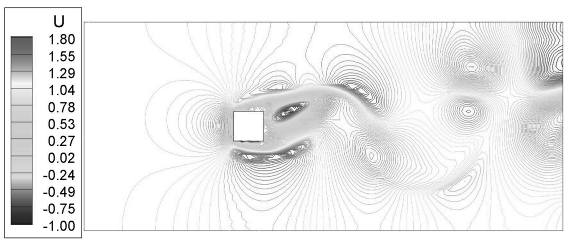

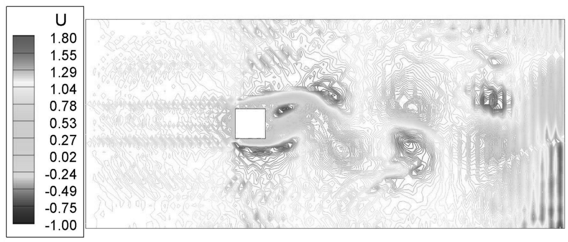

(a) Present method (b) LES without SUPG

Fig. 8 Streamwise velocity (u) field at t = 100 for Re = 22000

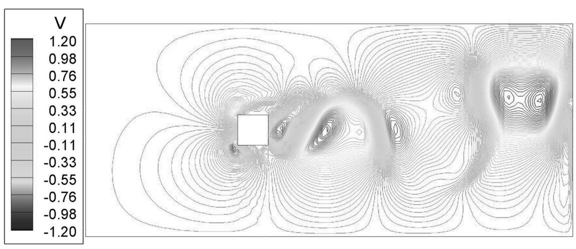

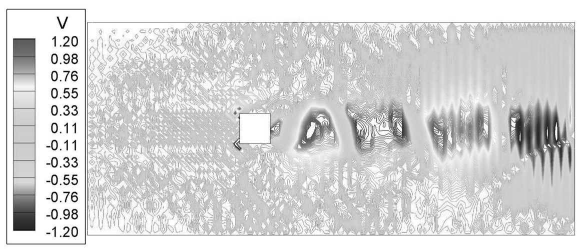

(a) Present method (b) LES without SUPG

Fig. 9 Lateral velocity (v) field at t = 100 for Re = 22000

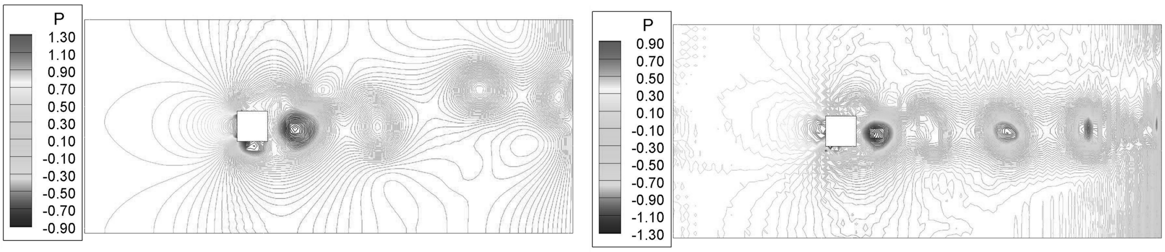

(a) Present method (b) LES with SUPG

Fig. 10 Pressure (p) field at t = 100 for Re = 22000

$$S_t = (H)/(UT) \tag{25}$$

where F_d and F_l are the drag and lift forces, T is the vortex shedding period.

Fig. 11(a) and (b) show the time history and the power spectrum of drag coefficient (C_d). It can be seen that the fluctuation of the drag coefficient (C_d) has an unalterable mean value unequal to zero and there are more than one key frequency components in the power spectrum of drag coefficient (C_d). Figs. 12(a) and (b) show the time history and the power spectrum of lift coefficient (C_l). Obviously it can be seen that the fluctuation of the lift coefficient (C_l) has a mean value equal

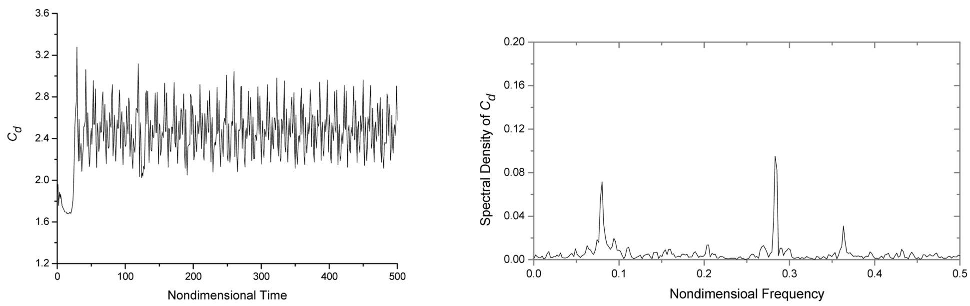

(a) time history of drag coefficient (C_D) (b) power spectrum of drag coefficient (C_d)

Fig. 11 Time history and power spectrum of drag coefficient (C_d) for Re = 22000

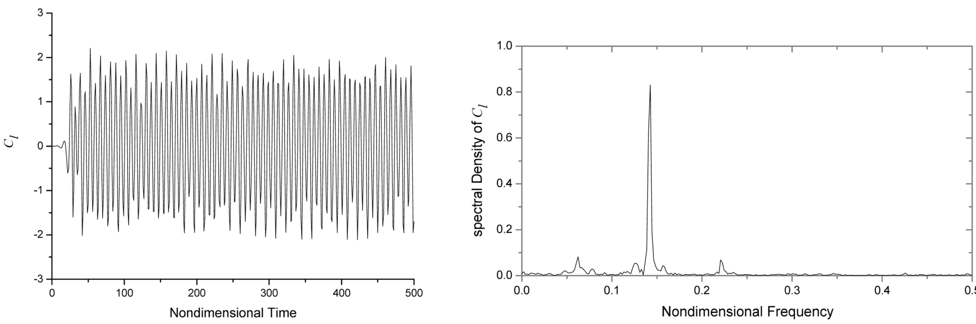

(a) time history of drag coefficient (C_l) (b) power spectrum of drag coefficient (C_l)

Fig. 12 Time history and power spectrum of lift coefficient (C_l) for Re = 22000

Table 1 Comparison of vortex shedding parameters with results of other references

	Computational cases		Re	S_t	C_d		C_l
					Mean	RMS	RMS
Present	2D LES	FEM	22000	0.142	2.44	0.20	1.03
Case A	2D LES	FEM	22000	0.147	2.02	0.11	0.87
Case B	2D LES	FEM	22000	0.137	2.31	0.26	1.15
Jeong and Koh (2002)	RNG k-ε	FEM	22000	0.144	2.39	-	-
Murakami and Mochida (1995)	2D LES	FEM	22000	0.132	2.09	-	-
Lee and Bienkiewicz (1998)	3D LES	FEM	22000	0.134	2.06	0.33	1.214
Lyn and Rodi (1989)	Exp.	-	22000	0.135	2.14	-	-
Durao *et al.* (1998)	Exp.	-	22000	0.139	-	-	-
Franke and Rodi (1993)	2D RSE	FVM	22000	0.136	2.15	-	-
Yu and Kareem (1997)	3D LES	FDM	100000	0.135	2.14	0.25	1.15

to zero and there is one main frequency component in the power spectrum of lift coefficient (C_l).

The time-averaged (mean) and RMS (root mean square) values of drag coefficient (C_d) and lift coefficient (C_l), and the Strouhal number S_t predicted by present computation are compared with the results from others in Table 1. For the verification of mesh independence, the results from other two cases are also shown. They are Case A containing 2775 rectangle elements with mesh size of 0.2, and Case B with 11000 rectangle elements, which mesh size is 0.1. It can be seen that the present method gains acceptable results compared with results from other researchers, and present predictions would become worse with the coarseness of the meshes.

4.2.3 Velocity fields analysis

The mean and RMS values of velocities at some typical positions are compared with the results from other researchers. The time-averaged (mean) value of the streamwise velocity (u) downstream of the square cylinder, along the plane of symmetry is compared with the numerical and experiment data from other researchers in Fig. 13. It can be seen that present results get a fairly close to the experiment data from Durao *et al.* (1998), which means that present prediction gets a right vortex shedding phenomena behind the square cylinder compared with experimental and numerical results.

The Fig. 14(a) and (b) show the RMS values of streamwise velocity (u) and lateral velocity (v) along centerline, downstream of cylinder. The RMS value of streamwise velocity (u) by the present method gets rough agreement with data from Lyn *et al*. (1995), but having a higher prediction in the field of $2H < x < 4H$ downstream of cylinder, which means that present method has exorbitant streamwise oscillation prediction in that field. The RMS value of lateral velocity (v) does not agree well with Lyn *et al*. (1995) in the area far from the cylinder, which means that present method gets exorbitant lateral oscillation prediction in the field of $x > 4H$.

Fig.15(a) and (b) compare the mean and RMS values of streamwise velocity(u) distribution from present results with data from others at the location 0.5H downstream of the leeward face of the cylinder. It can be seen that both the mean value and the RMS value of the streamwise velocity (u) from the present data agree well with the experimental data from Lyn *et al.* (1995) and Durao *et al.* (1998).

Fig. 16(a) and (b) compare the mean and RMS values of lateral velocity(v) distribution from

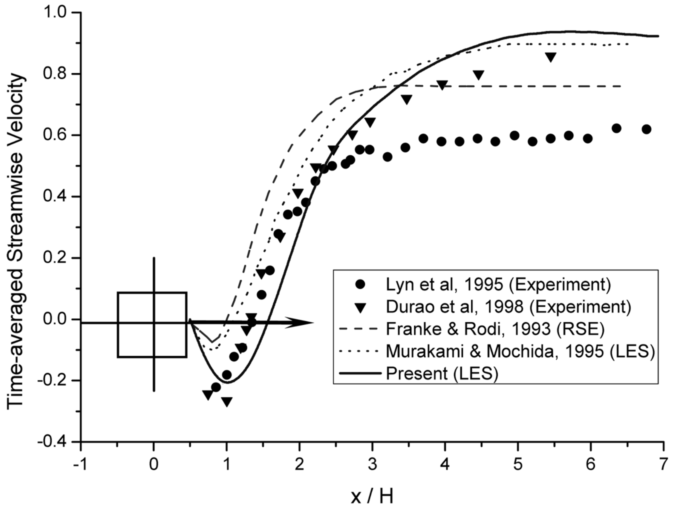

Fig. 13 Time-averaged streamwise velocity (u) along centerline, downstream of cylinder

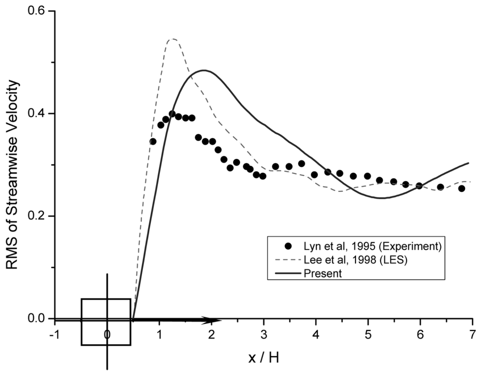

(a) streamwise Velocity (u)

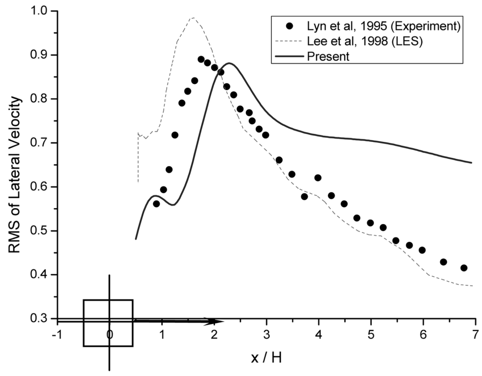

(b) lateral Velocity (v)

Fig. 14 RMS values of streamwise velocity (u) and lateral velocity (v) along centerline, downstream of cylinder

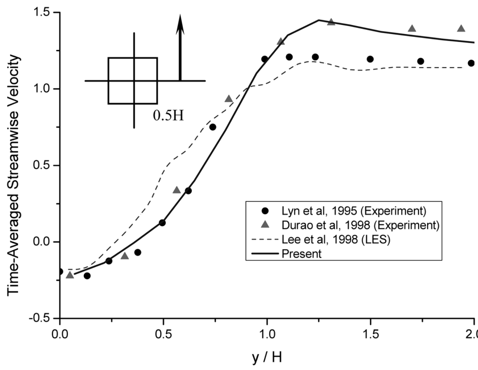

(a) time-averaged value

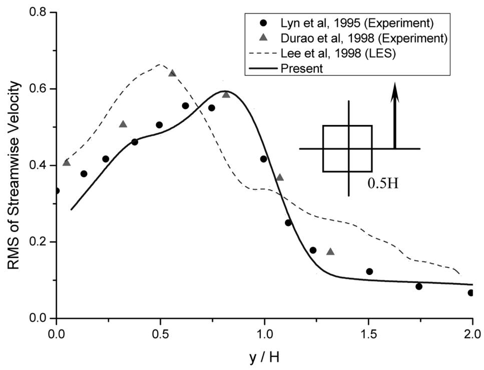

(b) RMS value

Fig. 15 Time-averaged and RMS values of streamwise velocity (u) profile

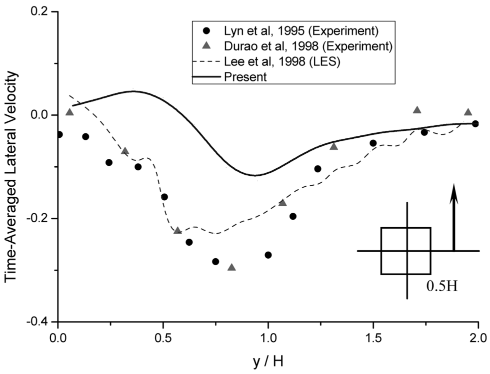

(a) time-averaged value

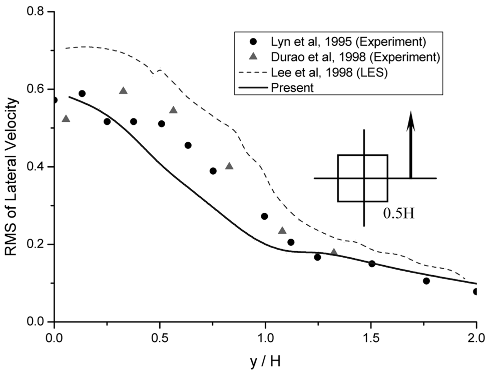

(b) RMS value

Fig. 16 Time-averaged and RMS values of lateral velocity (v) profile

present results with data from others at the location $0.5H$ downstream of the leeward face of the cylinder. We can see that the mean value of the lateral velocity (v) from the present data doesn't agree well with the experimental data near the cylinder but with right trend. Present prediction gets overestimate for mean lateral velocity in the field of $y < 1.0H$. And the present RMS value of lateral velocity (v) profile agrees reasonably with the experimental results but with a little discrepancy, which is acceptable compared with results form Lee *et al*. (1995).

Though there are differences between the experimental data and the results by present method, it is obvious that present results get acceptable prediction and right trend with the experimental data even with coarse mesh. And the present results could be closer to experimental data if finer mesh is applied. Thus the stabilization of present method and the capability of yielding to accurate prediction are testified.

5. Conclusions

This paper presents a stabilized finite element formulation for large eddy simulation to predict turbulent flow with high Reynolds number. In order to overcome the numerical oscillation caused by traditional FEM for solving turbulent flow, the SUPG stabilized form is implemented with the Smagorinsky sub-grid scale model to build the FEM weak equations of turbulent flow. And three-step technique is applied for temporal discretization. Then lid driven flow at $Re = 10^5$ in a triangular cavity and flow past square cylinder at $Re = 22000$ with coarse mesh are applied as numerical examples. Results show that present method can effectively suppress the computational instabilities of velocities and pressure fields, and yield to accurate prediction with coarse mesh for solving turbulent flow with high Reynolds number.

Acknowledgements

Support from the National Natural Science Foundation of China (No. 51078230), the Key Project of Fund of Science and Technology Development of Shanghai (No. 10JC1407900) and the Doctoral

Disciplinary Special Research Project of Chinese Ministry of Education (No. 200802480056) are acknowledged.

References

Bardina, J., Ferzuger, J.H. and Reynolds, W.C. (1980), "*Improved subgrid scale models for large eddy simulation*", AIAA paper, Fluid and Plasma Dynamics Conference.

Bao, Y., Zhou, D. and Zhao Y.J. (2010a), "A two-step Taylor-characteristic-based Galerkin method for incompressible flows and its application to flow over triangular cylinder with different incidence angles", *Int.J. Numer. Meth. Fl.*, **62**(11), 1181-1208.

Bao, Y., Zhou, D. and Huang, C. (2010b), "Numerical simulation of flow over three circular cylinders in equilateral arrangements at low Reynolds number by a second-order characteristic-based split finite element method", *Comput. Fluids*., 39(5), 882-899.

Becker, R. and Vexler, B. (2007), "Optimal control of the convection-diffusion equation using stabilized finite element methods" , *Numer. Math*., **106**(3), 349-367.

Brooks, A.N. and Hughes, T.J.R. (1982), "Streamline Upwind/Petrov Galerkin formulation for convection dominated flows with particular emphasis on the incompressible Navier-Stokes equations", *Comput. Method. Appl. M*., **32**(1), 199-259.

Buchan, A.G., Candy, A.S., Merton, S.R. and Pain, C.C. (2008), "The inner element sub-grid scale finite element method for the Boltzmann transport equation" , Preprint submitted to Elsevier.

Collis, S.S. and Heinkenschloss, M. (2002), "Analysis of the streamline Upwind/Petrov Galerkin method applied to the solution of optimal control problems", CAAM TR02-01, March.

Deardorff, J.W. (1970), "A numerical study of three-dimensional turbulent channel flow at large Reynolds numbers", *J. Fluid Mech*., **41**(2), 453-480.

Dettmer, W. and Peric, D. (2006), "A computational framework for fluid–structure interaction: Finite element formulation and applications", *Comput. Appl. M*., **195**(41), 5754-5779.

Donea, J., Giuliani, S., Laval, H. and Quartapelle, L. (1984), "Time-accurate solution of advection-diffusion problems", *Comput. Method. Appl. M*., **45**(1-3), 123-146.

Durao, D.F.G., Heitor, M.V. and Pereira, J.C.F. (1998), "Measurements of turbulent and periodic flows around a square cross-section cylinder", *Exp. Fluids*, **6**(5), 298-304.

Franca, L.P. and Frey, S.L. (1992), "Stabilized finite element methods: II. The incompressible Navier-Stokes equations", *Comput. Method. Appl. M*., **99**(2), 209-233.

Franke, R. and Rodi, W. (1993), "Calculation of vortex shedding past a square cylinder with various turbulent models", Turbulent Shear Flows VIII, 189-204.

Germano, M., Piomelli, U., Moin, P. and Cabot, W.H. (1991), "A dynamic subgrid-scale eddy viecosity model", *Phys. Fluid.*, **3**(7), 1760-1765.

Hasebe, H. and Nomura, T. (2009), "Finite element analysis of 2D turbulent flows using the logarithmic form of the k-å model", *Wind Struct*., **12**(1), 21-47.

Heinkenschloss, M. and Leykekhman, D. (2008), *Local error estimates for supg solutions of advectiondominated elliptic linear-quadratic optimal control problems* , Tech. Rep. TR08-30, Department of Computational and Applied Mathematics, Rice University.

Hughes, T.J.R., Franca, L.P. and Balestra, M (1986), "A new finite element formulation for computational fluid dynamics: V. Circumventing the Babuška-Brezzi condition: A stable Petrov-Galerkin formulation of the Stokes problem accommodating equal-order interpolations", *Comput. Method. Appl. M*., **59**(1), 85-99.

Hughes, T.J.R., Franca, L.P. and Hulbert, G.M. (1989), "A new finite element formulation for computational fluid dynamics: VIII, The Galerkin least-squares method for advective diffusive equations", *Comput. Method. Appl. M*., **73**(2), 173-189.

Itoh, Y. and Tamura, T. (2008), "Large eddy simulation of turbulent flows around bluff bodies in overlaid grid systems", *J. Wind Eng. Ind. Aerod*., **96**(10), 1938-1946.

Jeong, U.Y. and Koh, H.M. (2002), "Finite element formulation for the analysis of turbulent wind flow passing bluff structures using the RNG k-å model", *J. Wind Eng. Ind. Aerd*., **90**(3), 159-169.

Jiang, C.B. and Kawahara, M. (1993), "A three step finite element method for unsteady incompressible flows",

Comput. Mech., **11**(5), 355-370.
Jimenez, A., Crespo, A., Migoya, E. and Garcia, J. (2008), "Large-eddy simulation of spectral coherence in a wind turbine wake" , *Environ. Res. Lett*., **3**(1).
Lee, S. and Bienkiewicz, B. (1998), "Finite element implementation of large eddy simulation for separated flows", *J. Wind Eng. Ind. Aerod*., **77-78**(2), 603-617.
Lyn, D.A., Einav, S., Rodi, W. and Park, J.H. (1995), "A laser-Doppler velocimeter study of ensemble-averaged characteristics of the turbulent near wake of a square cylinder", *J. Fluid Mech*., **304**, 285-319.
Lyn, D.A. and Rodi, W. (1989), "Phase-averaged turbulence measurements in the separated shear region of flow around a square cylinder", *Proceedings of the 23th cong. Ind. Ass. Hydraulic Research*, Ottawa, August.
Ma, S.W., Song. L.F., Ong, S.L. and Ng, W.J. (2004), "A 2-D streamline upwind Petrov/Galerkin finite element model for concentration polarization in spiral wound reverse osmosis modules" , *J. Membrane Sci*., **244**(1-2), 129-139.
Murakami, S. and Mochida, A. (1995), "On turbulent vortex-shedding flow past 2D square cylinder predicted by CFD", *J. Wind Eng. Ind. Aerd*., **54-55**, 191-211.
Oñate, E. (1998), "Derivation of stabilized equations for advective-diffusive transport and fluid flow problems", *Comput. Method. Appl. M*., **151**(1), 233-267.
Pain, C.C., Eaton, M.D., Smedley-Stevenson, R.P. and Piggott, M.D. (2006), "Space-time streamline upwind Petrov-Galerkin method for the Boltzmann transport equation" , *Comput. Method. Appl. M*.,**195**(33-36), 4334-4357.
Ramakrishnan, S. and Collis, S.S., (2006), "Partition selection in multiscale turbulence modeling" , *Phys.Fluid*, **18**(7).
Selmin, V., Donea, J. and Quartapelle, L. (1985), "Finite element methods for nonlinear advection", *Comput. Method. Appl. M*., **52**(1-3), 817- 845.
Smagorinsky, T.S. (1963), "General circulation experiment with primitive equations: Part I, Basic experiments", *Mon. Weather Rev*., **91**, 99-164.
Tezduyar, T.E. (2007), "Finite elements in fluids: Stabilized formulations and moving boundaries and interfaces", *Comput. Fluids*, **36**(2), 191-206.
Tutar, M. and Celik, I. (2007), "Large eddy simulation of a square cylinder flow: Modelling of inflow turbulence.", *Wind Struct*., **10**(6), 511-532.
Uchida, T. and Ohya, Y. (2003), "Large-eddy simulation of turbulent airflow over complex terrain" , *J. Wind Eng. Ind. Aerod*., **91**(1-2), 219-229.
Yu, D.H. and Kareem, A. (1997), "Numerical simulation of flow around a rectangular prsim", *J. Wind Eng. Ind. Aerod*., **67-68**, 195-208.
Zienkiewicz, O.C. and Codina, R. (1995), "A general algorithm for compressible and incompressible flow. Part I: The split characteristic based scheme", *Int. J. Numer. Meth. Flu*., **20**(8), 869-885.

CC

List of symbols

u_i	i directional velocity
p	pressure
t	time
v	kinematic viscosity
v_t	turbulent eddy viscosity
Re	Reynolds number
ρ	density of fluid
k	SGS turbulent kinetic energy
S_{ij}	strain rate tensor
h	element volume size

C_S, C_k	parameters of LES
δu_i	velocity test function
n_j	normal unit vector
σ_{ij}	stress tensor
Γ	computational boundary
Ω	computational domain
Ω^e	element domain
n_{el}	number of elements
τ_{SUPG}	stabilized parameter of SUPG
h^e	characteristic size of an element
u^e	characteristic convective velocity of an element
Re^e	Reynolds number of an element
β_1, β_2, z	process parameters of SUPG
u_{iI}	i directional velocity of node I
p_I	pressure of node I
Φ_I	trial and test function of FEM
M, N, G, H, D, B	basis matrices of element for momentum equation
S, Q, R, T	basis matrices of element for pressure equation
U	characteristic velocity
H	characteristic length
u	horizontal velocity
v	vertical velocity
F_d	drag force
F_l	lift force
C_d	drag coefficient
C_l	lift coefficient
S_t	Strouhal number
T	vortex shedding period